Title

TOUGH-UDEC: A simulator for coupled multiphase fluid flows, heat transfers and discontinuous deformations in fractured porous media

Authors

Lee, Jaewon
Kim, Kwang-Il
Min, Ki-Bok
et al.

Publication Date

2019-05-01

DOI

10.1016/j.cageo.2019.02.004

Peer reviewed

TOUGH-UDEC: A Simulator for Coupled Multiphase Fluid Flows, Heat Transfers and Discontinuous Deformations in Fractured Porous Media

[1]Jaewon Lee[a], [2]Kwang-Il Kim[b], [3]Ki-Bok Min[b], [4]Jonny Rutqvist[c]

[a]Korea Atomic Energy Research Institute, Daejeon, Korea

[b]Department of Energy Resources Engineering, Seoul National University, Seoul, Korea

[c]Lawrence Berkeley National Laboratory, Berkeley, United States of America

*Corresponding author: Ki-Bok Min (kbmin@snu.ac.kr)

Address: Department of Energy Resources Engineering, Seoul National University

1 Gwanak-ro, Gwanak-gu, Seoul 151-744, Korea

Citation: *Lee J., Kim K.-I., Min K.-B. and Rutqvist J. TOUGH-UDEC: A Simulator for Coupled Multiphase Fluid Flows, Heat Transfers and Discontinuous Deformations in Fractured Porous Media. Computers and Geosciences 126, 120–130 (2019).*

ABSTRACT

A numerical simulator entitled TOUGH-UDEC is introduced for the analysis of coupled thermal-hydraulic-mechanical processes in fractured porous media. Two existing well-established codes, TOUGH2 and UDEC, are coupled to model multiphase fluid flows, heat transfers, and discontinuous deformations in fractured porous media by means of discrete fracture representation. TOUGH2 is widely used for the modeling of heat transfers and multiphase multicomponent fluid flows, and UDEC is a well-known distinct element code for rock mechanics. The two codes are solved sequentially, with coupling parameters passed to each equation at specific intervals. After solving thermal-hydraulic equations within the TOUGH2 code, pressure and temperature information is imported into the UDEC model. After solving the mechanical equation within the UDEC code the calculated fracture apertures are converted to the equivalent permeability and porosity values for a TOUGH2 flow analysis. The solution is calculated by iteratively following an explicit sequence for numerical efficiency. Verifications are presented to demonstrate the capabilities of the coupled TOUGH-UDEC simulator. Three application examples of (1) shear dilation due to increased pore pressure, (2) thermal stress and (3) CO_2 injection, show that the new simulator can be an effective tool for geoengineering applications involving shear activation of fractures and faults.

Keywords: Thermal-hydraulic-mechanical coupling simulator, Shear slip, Distinct Element Method

1. Introduction

Shear slip of rock fractures is a critical process in many applications of geological engineering, such as CO_2 geosequestration (Shukla et al., 2010; Zoback and Gorelick, 2012), enhanced geothermal systems (EGS) (De Simone et al., 2017; Xie and Min, 2017), shale-gas production (Rutqvist et al., 2015), and underground nuclear waste disposal (Min et al., 2013; Hudson et al., 2001). Shear slip can induce mechanical instability and enhanced fluid flow in fractures, possibly resulting in substantially enhanced permeability of a fractured rock mass unit (Min et al., 2004; Rutqvist, 2015). Shear slip can be caused by various mechanisms. For example, a pore pressure increase caused by a CO_2 injection into a reservoir for carbon geosequestration reduces the effective normal stress between two fracture surfaces, which may induce fracture shear slip (Hawkes et al., 2005). For a deep geological repository used to store high-level nuclear waste, heat is emitted by the decaying nuclear waste and thermal stress is generated due to the confined nature of the rock. The thermal stress alters the stress distribution throughout the rock mass, and shear slip may be triggered (Ghassemi et al., 2005; Min et al., 2013).

There are basic requirements and desired features of numerical codes for the adequate modeling of hydraulically or thermally induced shear slip, termed hydroshearing or thermoshearing, respectively (Cladouhos et al., 2009; Min et al., 2013). First, the numerical code should be able to model coupled thermal, hydraulic and mechanical processes in fractured porous rock. Second, it is critical for the coupled hydromechanical and thermomechanical behavior of fractures to be modeled accurately. Third, in certain applications, such as CO_2 geosequestration and geothermal energy extraction from high-temperature steam reservoirs, the modeling of multiphase and multicomponent fluid flow processes is required. However, most existing simulators for geological applications considering coupled THM phenomena are limited with regard to adequately modeling hydroshearing and thermoshearing. COMSOL Multiphysics (COMSOL, 2017), OpenGeoSys (Kolditz et al., 2012), CODE_BRIGHT (Olivella et al., 1996), FEHM (Zyvoloski et al., 1988) and FALCON (Podgorney et al., 2010) are examples of fully-coupled codes that can handle multiphase fluid flow and geomechanics, including coupled THM processes in geological media. They are based on continuum modeling approaches which cannot explicitly consider hydromechanical and thermomechanical fracture processes involving large

number of fractures. Other codes such as FLAC3D (Itasca, 2009), THAMES (Ohnishi and Kobayashi, 1996), ROCMAS (Noorishad et al., 1984), ABAQUS (Börgesson et al., 2001) are also based on a continuum approach with limited capabilities of considering complex fracture behavior and fracture networks. Although there are numerical codes capable of modeling the hydromechanical behavior of fractures explicitly, including codes based on the distinct element method (DEM) such as UDEC (Itasca, 2011), and PFC (Itasca, 2008), distinct deformation analysis (DDA) (Shi, 1988), or the numerical manifold method (Hu et al., 2017), the fluid flow is often limited to take place within the fractures and does not include multiphase and multicomponent fluid flow.

Programs with code-coupling have been frequently applied. Examples include a simulator linking the multiphase flow simulator TOUGH2 and the reactive transport simulator TOUGHREACT to geomechanics codes, such as FLAC3D (Rutqvist, 2011; Rutqvist et al., 2002; Taron et al., 2009). Sequential coupling of two codes offers a significant advantage due to its modularity, by which the fluid and the mechanical solver for the corresponding governing equations can be executed separately without much modification, which is particularly desirable in many practical applications (Xie and Wang, 2014). Additionally, the sequential coupling will typically be more rapid and less expensive to develop, and the modular construction approach allows for easier implementation of future advances in constitutive relationships or modeling structures (Settari and Mourits, 1998). Finally, existing codes for sequential coupling are already well tested and widely applied in their respective fields.

The purpose of this study is to present the development of a numerical simulator that explicitly conducts a systematic and quantitative analysis of the hydroshearing and thermoshearing of discrete fractures in a fractured porous medium. Two existing codes were linked to model coupled multiphase fluid flows, heat transport, and mechanical processes in a complex fractured rock mass. These are TOUGH2, a finite volume multiphase flow and heat transport code (Pruess et al., 2012), and UDEC, a DEM geomechanical code. The two codes are linked by means of sequential executions and data transfers through a coupling module. Two verification examples and three application cases are presented using the developed TOUGH-UDEC simulator to demonstrate its capability to explicitly model shear slip-dilation behavior under coupled hydromechanical and thermomechanical processes.

2. Methodology

2.1. Mesh conversion from UDEC to TOUGH2

In order to link TOUGH2 and UDEC, the geometry and element numbering along fractures and matrix blocks should be consistent in the two codes. A special MATLAB routine was developed to produce finite volume mesh discretization for TOUGH2 based on the UDEC mesh. In TOUGH2, the numerical grid is defined into finite volume elements with one node located at the centroid of an element. In UDEC, mesh discretization includes zones within matrix blocks, and the domains within fractures and nodes are located at the corners of the zones (Fig. 1). The domains within fractures are defined as apertures between nodal points along the fractures (Fig. 1). These fracture domains are typically small compared to the zones within the matrix blocks, which can lead to numerical convergence problems and reduced time steps for the flow and heat calculation in TOUGH2. To mitigate such numerical problems, the fractures in TOUGH2 are represented by porous elements of a certain thickness larger than the physical aperture in UDEC, with equivalent permeability and effective porosity (Stephens et al., 1998) calculated from the UDEC facture aperture (Eqs. (1) and (2)).

$$k_e = \frac{e^3}{12b} \tag{1}$$

$$n_e = \frac{e}{b} \tag{2}$$

Where k_e is the equivalent permeability, n_e is the effective porosity, e denotes the hydraulic aperture, and b is the width of the TOUGH2 fracture elements.

2.2. Code-linking logic

When linking a fluid flow and geomechanical codes sequentially, four different operator-split strategies for the coupling scheme exist: two schemes in which the mechanical problem is solved first (drained and undrained splits) and two schemes where the fluid flow problem is solved first (fixed-strain and fixed-stress splits) (Kim et al., 2011). Among them, the solutions of fixed-stress splitting methods are unconditionally stable and the convergence properties are comparable to those of the fully coupled method (Kim et al., 2011). For TOUGH-UDEC coupled simulations, we applied the fixed-stress splitting method to achieve optimum stability and the best convergence rate.

For certain strongly coupled problems, there is likely a trade-off between the computational time and the degree of accuracy. According to Preisig and Prévost (2011), for strongly coupled poro-elastic problems, a sequential (or staggered) solution method could require a large number of iterations to attain the same results achievable with the fully coupled method. This indicates that sequential coupled methods could be less efficient than fully coupled methods. However, several recently published studies have shown that a fixed stress split is a robust and efficient scheme for iteratively coupling poro-elastic systems, even in the case of highly nonlinear and anisotropic problems (Mikelíc et al., 2014; White et al., 2016; Dana and Wheeler, 2018). Moreover, the type of coupling plays an important role, whether dominant by direct pore-volume couplings or indirect couplings through property changes (Rutqvist, 2017), as does the rate of change in the system. If coupling variables of the porosity and permeability change slowly, as in most geological engineering problems, or the time step is relatively small, the accuracy of the results is guaranteed even with relatively few iterations (Rutqvist et al., 2002; Rutqvist, 2017). Therefore, in TOUGH-UDEC, we apply an explicit sequential scheme for numerical efficiency, which means that the coupling variables of the porosity and permeability are evaluated only at the beginning of each time step, with TOUGH2 holding the time step size to a small value to avoid any abrupt change in the hydrological conditions.

A flow diagram of the explicit sequential coupling procedure used with TOUGH-UDEC is shown in Fig. 2. After solving thermal and hydraulic equations in TOUGH2 at a fixed level of stress, the

pressure (P) and temperature (T) are supplied to UDEC. Although calculation of the mechanical process is operated only at the corner nodes, the pressure is directly stored at the center of the zones and domains of UDEC. In the current version of UDEC, temperature data can only be stored at the corner nodes. Thus, temperature data transferred from the centroid of a mesh in TOUGH2 are interpolated at the corner nodes by considering the distance from each corner node to the centroid. If UDEC is updated to store the temperature at the centroid of a mesh in the future, the code will be modified. After solving the mechanical equations in UDEC, the updated aperture (e) of each fracture is converted to the permeability (k_e) and porosity (n_e) and used for the fluid flow calculation in TOUGH2. The solution is calculated by iteratively following an explicit sequence.

2.3. Verifications

TOUGH2 and UDEC have each been extensively verified, i.e., TOUGH2 (Pruess et al., 2012) for multiphase (gas and liquid) fluid flows and heat transport (conductive and convective) and UDEC (Itasca, 2011) for geomechanics, including solid rock and fracture mechanical behavior. Moreover, both TOUGH2 and UDEC have a large user base, thus providing additional confidence with regard to their validity and applicability (Lee et al., 2015). Accordingly, our verification presented in this section is focused on the coupling between TOUGH2 and UDEC. Two independent code verifications were conducted relevant to code linking and coupled hydromechanical and thermomechanical responses in reservoirs.

2.3.1. Uniaxial consolidation

For the hydromechanical response, a uniaxial consolidation analysis was conducted and the numerical results were compared with Terzaghi's analytic solution for this problem (Terzaghi, 1923). Fig. 3 shows a schematic view of the numerical model. The initial and boundary conditions are represented using the vertical lines with the specified depth of the model. Table 1 shows the properties

used for the verification.

If mechanical loading (σ_m) is applied at the upper boundary of one-dimensional saturated poroelastic media with height h, the pore pressure (P_p) at height z and time t is given as follows (Jaeger et al., 2007):

$$P_p(z,t) = \frac{\alpha M \sigma_m}{(\lambda+2G+\alpha^2 M)} \sum_{n=1,3,\cdots}^{\infty} \frac{4}{n\pi} sin\left(\frac{n\pi z}{2h}\right) exp(-\frac{n^2\pi^2 kt)}{4\mu Sh^2}), \quad (3)$$

where α is the Biot constant, M is the Biot modulus, λ is the Lamé constant, G is the shear modulus, k denotes the permeability, μ is the fluid viscosity, and S is the storage coefficient.

The vertical displacement (w) at the upper boundary (z = 0 m) versus time is determined as follows:

$$w(0,t) = \frac{-\sigma_m h}{(\lambda+2G)}\left[1 - \frac{\alpha^2 M}{(\lambda+2G+\alpha^2 M)} \sum_{n=1,3,\cdots}^{\infty} \frac{8}{n^2\pi^2} \exp(-\frac{n^2\pi^2 kt)}{4\mu Sh^2})\right] \quad (4)$$

Fig. 4 (a), (b), and (c) show the evolution of the pressure at the lower boundary, the evolution of the displacement at the upper boundary, and the pressure distributions after 10^5, 10^6, and 10^7 seconds. The numerical results are in close agreement with the analytical solutions.

2.3.2. Heating of a hollow cylinder

To verify the algorithms and code implementations related to thermomechanical responses, the heating of a hollow cylinder simulation was conducted for a comparison with analytic solutions. Nowacki (1962) provides the solution to this problem in terms of the temperatures and radial, tangential and axial stresses in a steady state, as shown below.

$$\frac{T(r)}{T_a} = \frac{\ln(b/r)}{\ln(b/a)} \quad (5)$$

$$\frac{\sigma_r(r)}{mGT_a} = -\left[\frac{\ln(b/r)}{\ln(b/a)} - \frac{(b/r)^2 - 1}{(b/a)^2 - 1}\right] \tag{6}$$

$$\frac{\sigma_t(r)}{mGT_a} = -\left[\frac{\ln(b/r) - 1}{\ln(b/a)} + \frac{(b/r)^2 + 1}{(b/a)^2 - 1}\right] \tag{7}$$

$$\frac{\sigma_a(r)}{mGT_a} = -\left[\frac{2\ln(b/r) - \frac{\lambda}{2(\lambda + G)}}{\ln(b/a)} + \left(\frac{\lambda}{2\lambda + G}\right)\left(\frac{2}{(b/a)^2 - 1}\right)\right] \tag{8}$$

Where $m=3K\alpha_T/(\lambda+2G)$, $\lambda=K-2G/3$, r is the radial distance from the cylinder center, a is the inner radius of the cylinder, b is the outer radius of the cylinder, T_a is the temperature at the inner radius, σ_r is the radial stress, σ_t is the tangential stress, σ_a is the axial stress, K is the bulk modulus, G is the shear modulus, and α_T is the linear thermal expansion coefficient.

A quarter section of the cylinder is modeled, and Fig. 5 shows the geometry and boundary conditions. A constant-temperature boundary of 100 °C is specified at the inner radius of the model. The temperature at the outer radius is set to 0 °C. Table 2 presents the properties of the model.

Fig. 6 shows the temperature contour of the model in a steady state, and Fig. 7 shows the temperature, radial stress, tangential stress, and axial stress distributions along the radial axis AA' in Fig. 5 compared with those of the analytic solutions. The plotted values are normalized, in which the temperature and stress are normalized by T_a and mGT_a, respectively. The results of the numerical analysis are in good agreement with those of the analytical solutions showing that the data transfer and coupling between TOUGH and UDEC is working properly.

3. Applications

3.1. Fluid injection into a single inclined joint

In order to demonstrate the capability of the explicit modeling of the transient hydromechanical behavior of a joint, a simulation was conducted in which fluid is injected into a single inclined joint. Fig. 8 shows the model geometry. The initial and boundary conditions are represented using the inclined or vertical (if the variable is constant) lines with the specified depth of the model. Table 3 presents the material properties. Water is injected along the joint at a flow rate of 0.8 kg/s to build up the pore pressure uniformly. The normal and shear stiffness of the joint are held constant. A Coulomb slip criterion is used to determine the condition of shear failure.

Fig. 9 shows the variation of the pore pressure, aperture, shear displacement and stress state at the center of the joint before the injection and after 260 seconds of the injection. Due to the constant injection rate, the pressure increases linearly from 9.8 MPa to 20.3 MPa (Fig. 9 (a)). The stress state reached failure after 170 seconds of injection (Fig. 9 (c)), after which shear slip started to occur (Fig. 9 (b)). Before shear slip, the aperture of the joint initially increased as a result of the reduced effective normal stress. After the shear slip, shear dilation gives rise to an additional normal displacement until the shear displacement reaches the critical shear displacement for a dilation of 5 mm, with this value taken from (McClure and Horne, 2011). The numerical result of the aperture is in good agreement with the analytic solution (Esaki et al., 1999; Min et al., 2004), as presented below.

$$e = e_0 + \frac{\Delta\sigma_n'}{k_n} + \tan(\theta) * \Delta\delta_s \tag{9}$$

Where e is the aperture, e_0 represents the initial aperture, σ'_n is the effective normal stress, k_n is the normal stiffness, θ is the dilation angle, and δ_s is the shear displacement. The aperture of the joint increased by six-fold after 260 seconds of the injection.

3.2. Cooling around a single inclined joint

In order to demonstrate the capability of the explicit modeling of the transient thermomechanical behavior of joints, heat extraction is conducted at a single inclined joint. Fig. 10 shows the model geometry and initial and boundary conditions, and Table 4 presents the material properties. Heat is extracted along the joint at a rate of -1,200 J/s. The normal and shear stiffnesses are held constant. A Coulomb slip criterion is used to determine the condition of shear failure.

The temperature at the center of the joint decreases from 100 °C to 29.8 °C (Fig. 11 (a)). Initially, the aperture of the joint increases gradually due to changes in the cooling-induced normal stress (Fig. 11 (b) and (c)). The stress state at the center of the joint reaches failure after one year of heat extraction, and shear displacement then increases sharply (Fig. 11 (b) and (c)). After the initiation of shear slip, the aperture of the joint also increases, mostly due to shear dilation. The numerical result of the aperture is in good agreement with the analytic solution according to Eq. (9). The aperture of the joint increased by 5.3 times after three years.

3.3. Large-scale CO_2 injection and leakage analysis

The TOUGH-UDEC simulator was applied to a large scale domain to demonstrate its capability for modeling CO_2 geosequestration into a brine formation. Due to buoyancy of CO_2 with a density of 200-900 kg/m^3, which is lower than that of brine, the integrity of the caprock is crucial to avert the leakage of injected CO_2 for a sufficiently long period (Rutqvist et al., 2002). In order to investigate the aperture change of a fault due to shear slip, a numerical analysis with a particular TOUGH2 module for brine-CO_2 mixtures was conducted in the current study (Pruess and Garcia, 2002).

The schematic geometry and initial and boundary conditions are shown in Fig. 12. The formation temperature was held constant as hydro-mechanical coupling was considered to be sufficient to investigate the change in the aperture. CO_2 was injected at the bottom of a 200-m-thick sandstone

aquifer, and the injection rate per meter (normal to model) is consistent with that of the In Salah, Algeria CCS site considering the 1 – 1.5 km length of horizontal injection wells (Rutqvist et al., 2010). The formation properties, including the relative permeability and capillary pressure functions of the model, was taken from those used in Rutqvist et al (2010) (Table 5). The single fault is located across the shale caprock slightly straddling the overburden and injection layers. In order to represent the effects of shear slip, two cases with identical conditions except for the friction angle of the fault were compared (Table 6).

Fig. 13 shows the variations of the pore pressure, aperture, and shear displacement at the top, center, and bottom of the fault for cases 1 and 2. Due to the CO_2 injection, the pore pressure at the center and bottom of the fault starts to increase, whereas the pore pressure at the top of the fault remains nearly constant in both cases. After approximately 0.15 years of injection, shear slip occurs locally at the bottom of the fault for case 1, which locally affects the aperture and effectively results in a significant increase in the fault permeability (Fig. 13 (c)). After about 0.85 years of injection, shear slip extends along the entire fault, inducing an abrupt increase of the aperture along the entire fault. The pore pressures at the top and middle of the fault become equal to that at the bottom of the fault after this abrupt shear slip event. In case 2, shear slip does not occur owing to the higher shear strength.

Aperture profiles along the depth of the fault after two years of injection are shown in Fig. 14. In case 1, the aperture of the fault increases much more than it does in case 2, as shear dilation significantly affects the aperture of the fault. In case 2, only normal deformation due to the pore pressure affects the aperture. The CO_2 gas saturation contour during the formation of both cases shows that the integrity of the caprock was compromised by the shear slip, through which CO_2 leakage could occur (Fig. 15).

This application example demonstrates the capability of the TOUGH-UDEC simulator to study the large-scale hydromechanical behavior of a fault with explicit modeling of shear slip across a fault represented by a discontinuity, which can contribute to the understanding of the critical mechanisms related to the long-term storage security of a large-scale CO_2 injection project. Other fluid injection applications involving deformation in discontinuities, such as hydraulic stimulations in EGS, will be considered in future studies.

4. Discussion

The merit of the TOUGH-UDEC simulator is its capability to undertake the explicit modeling of fracture behaviors driven by hydraulic and thermal processes in systems of fractured and porous media. Earlier THM coupled simulators using continuum-based models represent the fracture element using relatively thin continuum elements and typically use the empirical stress versus permeability functions (Rutqvist et al., 2002). Continuum-based fracture representation is limited in that it can only be applied to the complex fracture networks observed in many engineering applications related to the THM behavior of subsurface rocks, such as EGS, CO_2 geosequestration, and underground nuclear waste disposal (Lei et al., 2017). The TOUGH-UDEC simulator may be applicable to multiple fracture models due to its explicit consideration of the fracture system.

The current simulator has the following limitations. First, the TOUGH-UDEC simulator is not able to consider the influences of fault-filling materials on the fault behavior. Variation of the gouges and clays during shear slip could affect the friction coefficients (Numelin et al., 2007). The permeability of the fault could change during the long-term CO_2 injection operation due to the chemical reactions of clays and minerals (Rochelle et al., 2004). Such chemical reactions could be managed if a coupled simulator between UDEC and TOUGHREACT, which is an extended version of TOUGH2 for chemically reactive transport, were to be developed. Second, the convective heat transfer between fluid and rock currently available in TOUGH (Moridis and Pruess, 1992; Pruess et al., 2012) is not fully implemented into the TOUGH-UDEC simulator; this would allow for the convective heat transfers in the fractures within rock masses. Third, the generation and propagation of a fracture cannot be modeled, and the current TOUGH-UDEC simulator is limited in applications involving the generation and propagation of certain types of fractures, such as hydraulic fracturing in a shale gas reservoir, and mixed-mechanism stimulations in an EGS reservoir (McClure and Horne, 2014). Fourth, the porosity in Eq. (2) should be applied to isotropic materials. The anisotropic characteristics of the porosity resulting from the pore connectivity as indicated in several numerical and field studies (Blum et al., 2009; Endo et al., 1984; Neuman, 2005) can be considered in future studies.

It was noted that the numerical demonstration of CO_2 leakage presented here must be interpreted

with caution due to the potential for more complex fault characteristics. The loss of caprock integrity in section 3.3 occurred due to a change in the permeability along a single and homogeneous fault as a result of changes in the effective normal stress and shear dilation. In reality, however, other factors also contribute to caprock integrity. First, a fault in a low-permeable formation with high clay content tends to retain fault-filling materials such as gouge, clay, and minerals. The permeability of such faults could be very low, even after shear slip, comparable to that before the shear slip (Laurich et al., 2014; Vilarrasa and Makhnenko, 2017). Second, shale formations or clay-rich faults could have high capillary entry pressure levels on the order of several MPa (Vilarrasa and Makhnenko, 2017; Espinoza and Santamarina, 2017). In section 3.3, the capillary entry pressure of the shale caprock is 1.1 MPa, but that of the fault is 6.7 kPa, which is set low to highlight the effect of shear slip on the leakage of CO_2. Considering that the CO_2 overpressure for cases 1 and 2 is less than 1 MPa within two years of the injection, CO_2 leakage would be restricted even after shear slip if the capillary entry pressure of the fault was assumed to be several MPa, Third, the hydraulic and mechanical heterogeneity along the faults affects the pore pressure diffusion (Rinaldi et al., 2014). Some regions with lower permeability could prevent the pressure from diffusing upward, resulting in a restricted area of fault activation and a relatively minor permeability increase of the fault.

5. Conclusions

In order to model the hydroshearing and thermoshearing of discrete fractures in fractured porous media, the TOUGH-UDEC simulator was developed. The current status of this development along with two verification examples and three applications are presented. The main contents are summarized as follows.

- Two existing well-established codes, TOUGH2 and UDEC, are linked to model coupled thermal, hydraulic and mechanical processes in fractured porous rock, with discrete fracture representation. A mesh conversion routine was developed to generate consistent model geometries and element numbering for both codes.

- The coupled equations are solved sequentially with coupling parameters passed to each equation at specific intervals. TOUGH2 solves thermal and hydraulic equations, and pressure and temperature are supplied to UDEC. After solving mechanical equations in UDEC, the updated permeability and porosity of the fracture are used for the fluid flow calculation in TOUGH2. The TOUGH-UDEC simulator was verified by two hydromechanical and thermomechanical verification cases, resulting in good agreement with analytical solutions.
- TOUGH-UDEC was applied to two basic hydroshearing and thermoshearing models with an inclined joint. The numerical result of the variation of the aperture matches the analytic solution well.
- The developed simulator was finally applied to a large-scale CO_2 injection and leakage analysis. Two cases with identical conditions except for the friction angle of the fault were compared. The case with a lower friction angle results in a much larger shear-dilation-induced aperture increase and greater CO_2 leakage compared to the other case with a higher friction angle. This application example demonstrates the applicability of the TOUGH-UDEC simulator for studying the large-scale hydromechanical behavior of a fault with the explicit modeling of shear slip across a fault represented by a discontinuity, and it can enhance the understanding of the critical mechanisms pertaining to the long-term stability of a large-scale CO_2 injection project.

Acknowledgement

This research was supported by the Nuclear Research and Development Program of the National Research Foundation of Korea (NRF-2017M2A8A5014857) funded by the Ministry of Science and ICT and by a grant from the National Research Foundation of Korea (NRF) funded by the Korean government (MSIP) (No. NRF-2015K1A3A7A03074226). Institute of Engineering Research at Seoul National University is acknowledged for the support on the manuscript preparation. Additional funding

to the LBNL author was provided by the U.S. Department of Energy to LBNL under contract No. DE-AC02-05CH11231.

References

Blum, P., Mackay, R., Riley, M.S., 2009. Stochastic simulations of regional scale advective transport in fractured rock masses using block upscaled hydro-mechanical rock property data. Journal of Hydrology 369, 318-325.

Börgesson, L., Chijimatsu, M., Fujita, T., Nguyen, T.S., Rutqvist, J., Jing, L., 2001. Thermo-hydro-mechanical characterisation of a bentonite-based buffer material by laboratory tests and numerical back analyses. International Journal of Rock Mechanics and Mining Sciences 38(1), 95–104.

Cladouhos, T., Petty, S., Larson, B., LIovenitti, J., Livesay, B., Baria, R., 2009. Toward more efficient heat mining: A planned Enhanced Geothermal System demonstration project. Geothermal Research Council Transactions 33, 165–70.

COMSOL, 2017. COMSOL Multiphysics Reference Manual version 5.3.

Dana, S., Wheeler M.F., 2018. Convergence analysis of fixed stress split iterative scheme for anisotropic poroelasticity with tensor Biot parameter. Computational Geosciences 22, 1219-1230.

De Simone, S., Carrera, J., Vilarrasa, V., 2017. Superposition approach to understand triggering mechanisms of post-injection induced seismicity. Geothermics 70, 85-97.

Endo, H.K., Long, J.C.S, Wilson, C.R., Witherspoon, P.A., 1984. A model for investigating mechanical transport in fracture networks. Water Resources Research 20(10), 1390-1400.

Esaki, T., Du, S., Mitani, Y., Ikusada, K., Jing, L., 1999, Development of a shear-flow test apparatus and determination of coupled properties for a single rock joint. International Journal of Rock Mechanics and Mining Sciences 36, 641-650.

Espinoza, D.N., Santamarina, J.C., 2017. CO_2 breakthrough – Caprock sealing efficiency and integrity for carbon geological storage. International Journal of Greenhouse Gas Control 66, 218-229.

Ghassemi, A., Tarasovs, S., Cheng, A.H.-D., 2005. Integral equation solution of heat extraction-induced thermal stress in enhanced geothermal reservoirs. International Journal for Numerical and Analytical Methods in Geomechanics 29, 829-844.

Hawkes, C.D., McLellan, P.J., Bachu, S., 2005. Geomechanical factors affecting geological storage of CO_2 in depleted oil and gas reservoirs. Journal of Canadian Petroleum Technology 44, 52–61.

Hu, M., Rutqvist, J, Wang, Y., 2017. A numerical manifold method model for analyzing fully coupled hydro-mechanical processes in porous rock masses with discrete fractures. Advanced in Water Resources 102, 111-126.

Hudson, J.A., Stephansson, O., Andersson, J., Tsang, C.F., Jing, L., 2011. Coupled T–H–M issues relating to radioactive waste repository design and performance. International Journal of Rock Mechanics and Mining Sciences 38(1), 143–161.

Itasca, 2008. PFC Manual: Particle Flow Code version 4.0. .Itasca Consulting Group Inc,

Minneapolis, Minnesota.

Itasca, 2009. FLAC-3D Manual: Fast Lagrangian Analysis of Continua in 3 Dimensions version 4.0. Itasca Consulting Group Inc, Minneapolis, Minnesota.

Itasca, 2011. UDEC Manual: Universal Distinct Element Code version 5.0. Itasca Consulting Group Inc, Minneapolis, Minnesota.

Jaeger, J.C., Cook, N.G.W., Zimmerman, R.W., 2007. Fundamentals of rock mechanics, 4th edn. Blackwell, London.

Kim, J., Tchelepi, H.A., Juanes, R., 2011. Stability, Accuracy, and Efficiency of Sequential Methods for Coupled Flow and Geomechanics. Society of Petroleum Engineers Journal 16(2), 249–262.

Kolditz, O., Bauer, S., Bilke, L., Böttcher, N., Delfs, J.O., Fischer, T. et al., 2012. OpenGeoSys: an open-source initiative for numerical simulation of thermo-hydro-mechanical/chemical (THM/C) processes in porous media. Environmental Earth Sciences 67. 589–599.

Laurich, B., Urai, J.L., Desbois, G., Vollmer, C., Nussbaum, C., 2014. Microstructural evolution of an incipient fault zone in Opalinus Clay: Insights from an optical and electron microscopic study of ion-beam polished samples from the Main Fault in the Mt-Terri underground research laboratory. Journal of Structural Geology 67. 107-128.

Lee, J.W., Min K.B., Rutqvist, J., 2015. TOUGH-UDEC simulator for the coupled multiphase fluid flow, heat transfer, and deformation in fractured porous media. In: 13th ISRM Congress, Montreal, Canada, paper No. 555. pp. 1-10.

Lei, Q., Latham, J.P., Tsang, C.F., 2017. The use of discrete fracture networks for modelling coupled geomechanical and hydrological behaviour of fractured rocks. Computers and Geotechnics 85, 151-176.

McClure, M.W., Horne, R.N., 2011. Investigation of injection-induced seismicity using a coupled fluid flow and rate/state friction model. Geophysics 76(6), WC181–WC198.

McClure, M.W., Horne, R.N., 2014. An investigation of stimulation mechanisms in Enhanced Geothermal Systems. International Journal of Rock Mechanics and Mining Sciences 72, 242–260.

Mikelíc, A., Wang, B., Wheeler, M.F., 2014. Numerical convergence study of iterative coupling for coupled flow and geomechanics. Computers & Geosciences 18, 325–341.

Min, K.B., Rutqvist, J., Tsang, C.F., Jing, L., 2004. Stress-dependent permeability of fractured rock masses: a numerical study. International Journal of Rock Mechanics and Mining Sciences 41, 1191–1210.

Min, K.B., Lee, J., Stephansson, O., 2013. Implications of thermally-induced fracture slip and permeability change on the long-term performance of a deep geological repository. International Journal of Rock Mechanics and Mining Sciences 61, 175–288.

Moridis, G., Pruess, K., 1992. TOUGH simulations of Updegraff's set of fluid and heat flow problems. Lawrence Berkeley Laboratory Report LBL-32611, Berkeley, California.

Neuman, S.P., 2005. On the tensorial nature of advective porosity. Advances in Water Resources 28(2), 149-159.

Noorishad, J., Tsang, C.F., Witherspoon, P.A., 1984. Coupled thermal-hydraulic-mechanical phenomena in saturated fractured porous rocks: Numerical approach. Journal of Geophysical Research: Solid Earth 89(B12), 10365–10373.

Nowacki, B.W., 1962. Thermoelasticity, Addison-Wesley Pub. Co., Reading.

Numelin, T., Marone, C., Kirby, E., 2007. Frictional properties of natural fault gouge from a low-angle normal fault, Panamint Valley, California, Tectonics 26 (2), 1-14.

Ohnishi, Y., Kobayashi, A., 1996. THAMES. In: Stephansson, O., Jing, L., Tsang, C.F. (Eds.), Coupled thermo-hydro-mechanical processes of fractured media. Developments in Geotechnical Engineering 79, 545–549.

Olivella, S., Gens, A., Carrera, J., Alonso, E.E., 1996. Numerical formulation for a simulator (CODE_BRIGHT) for the coupled analysis of saline media. Engineering Computations 13(7), 87–112.

Podgorney, R., Huang, H., Gaston, D., 2010. Massively parallel fully coupled implicit modeling of coupled thermal-hydrological-mechanical processes for enhanced geothermal system reservoirs. Proceedings, In: Thirty-Fifth Workshop on Geothermal Reservoir Engineering, Stanford University, Stanford, California, paper No. SGP-TR-188.

Preisig, M., Prévost, J.H., 2011. Coupled multi-phase thermo-poromechanical effects. Case study: CO_2 injection at In Salah, Algeria. International Journal of Greenhouse Gas Control 5(4), 1055-1064.

Pruess, K., Garcia, J., 2002. Multiphase flow dynamics during CO_2 disposal into saline aquifers. Environmental Geology 42, 282–295.

Pruess, K., Oldenburg, C., Moridis, G., 2012. TOUGH2 user's guide, Version 2.1. Lawrence Berkeley National Laboratory Report LBNL–43134, Berkeley, California.

Rinaldi, A.P., Jeanne, P., Rutqvist, J., Cappa, F., Guglielmi, Y., 2014. Effects of fault-zone architecture on earthquake magnitude and gas leakage related to CO_2 injection in a multi-layered sedimentary system. Greenhouse Gases: Science and Technology 4(1), 99-120.

Rochelle, C.A., Czernichowski-Lauriol, I., Milodowski, A.E., 2004, The impact of chemical reactions on CO_2 storage in geological formations: a brief review. Geological Society London Special Publications 233(1), 87-106.

Rutqvist, J., 2011. Status of the TOUGH-FLAC simulator and recent applications related to coupled fluid flow and crustal deformations. Computers & Geosciences 37, 739–750.

Rutqvist, J. 2017. An overview of TOUGH-based geomechanics models, Computers and Geosciences, 108, 56–63.

Rutqvist, J., 2015. Fractured rock stress-permeability relationships from in situ data and effects of temperature and chemical-mechanical couplings. Geofluids 15, 48–66.

Rutqvist, J. Vasco, D.W., Myer, L., 2010. Coupled reservoir-geomechanical analysis of CO_2 injection and ground deformations at In Salah, Algeria. International Journal of Greenhouse Gas Control 4, 225–230.

Rutqvist, J., Rinaldi, A.P., Cappa, F., Moridis, G.J., 2015. Modeling of fault activation and seismicity by injection directly into a fault zone associated with hydraulic fracturing of shale-gas

reservoirs. Journal of Petroleum Science and Engineering 127, 377–386.

Rutqvist, J., Wu, Y.-S., Tsang, C.-F., Bodvarsson, G., 2002. A modeling approach for analysis of coupled multiphase fluid flow, heat transfer, and deformation in fractured porous rock. International Journal of Rock Mechanics and Mining Sciences 39, 429–442.

Settari, A., Mourits, F., 1998. A coupled reservoir and geomechanical simulation system. Society of Petroleum Engineers (SPE) Journal 3, 219–226.

Shi, G.H., 1988. Discontinuous deformation analysis: a new numerical model for the statics and dynamics of block system. Ph. D. thesis, Department of Civil Engineering, University of California, Berkeley.

Shukla, R., Ranjith, P., Haque, A., Choi, X., 2010. A review of studies on CO_2 sequestration and caprock integrity. Fuel 89, 2651–2664.

Stephens, D.B., Hsu, K.C., Prieksat, M.A., Ankeny, M.D., Blandford, N., Roth, T.L., Kelsey J.A., Whitworth, J.R., 1998. A comparison of estimated and calculated effective porosity. Hydrogeology Journal 6, 156-165.

Taron, J., Elsworth, D., Min, K.B., 2009. Numerical simulation of thermal-hydrologic-mechanical-chemical processes in deformable fractured porous media. International Journal of Rock Mechanics and Mining Sciences 46(5), 842–854.

Terzaghi, K., 1923. Die Berechnung der Durchlassigkeitsziffer des Tones aus dem Verlauf der hydrodynamischen Spannungserscheinungen. Sber Akad Wiss, Wien Math Naturwiss Kl Abt II A 132, 125–138.

Vilarrasa, V., Makhnenko, R.Y., 2017. Caprock integrity and induced seimicity from laboratory and numerical experiments. Energy Procedia 125, 494-503.

White, J.A., Castelletto, N., Tchelepi H.A., 2016. Block-partitioned solvers for coupled poromechanics: A unified framework. Computational Methods in Applied Mechanical Enginerering 303, 55–74.

Xie, L., Min, K.B., 2017. Hydraulic fracturing initiation and propagation in deep inclined open hole for Enhanced Geothermal System. Geothermics 70, 351–366.

Xie, Y., Wang, G., 2014. A stabilized iterative scheme for coupled hydro-mechanical systems using reproducing kernel particle method. International Journal for Numerical Methods in Engineering 99, 819–843.

Zoback, M.D., Gorelick, S.M., 2012. Earthquake triggering and large-scale geologic storage of carbon dioxide. Proceedings of the National Academy of Sciences 109(26), 10164–10168.

Zyvoloski, G.A., Dash, Z.V., Kelkar, S., 1988. FEHM: Finite Element Heat and Mass transfer code. Los Alamos National Laboratory report. LA-11224-MS.

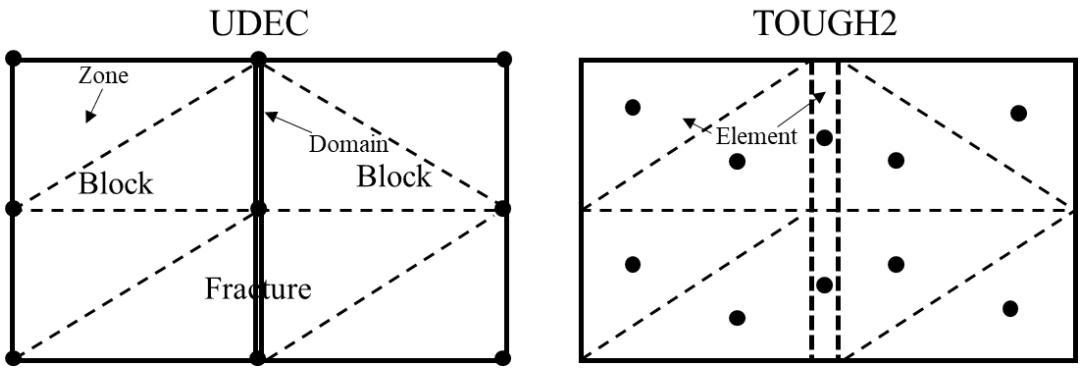

Fig. 1. Schematic view of basic mesh structures in UDEC and TOUGH2

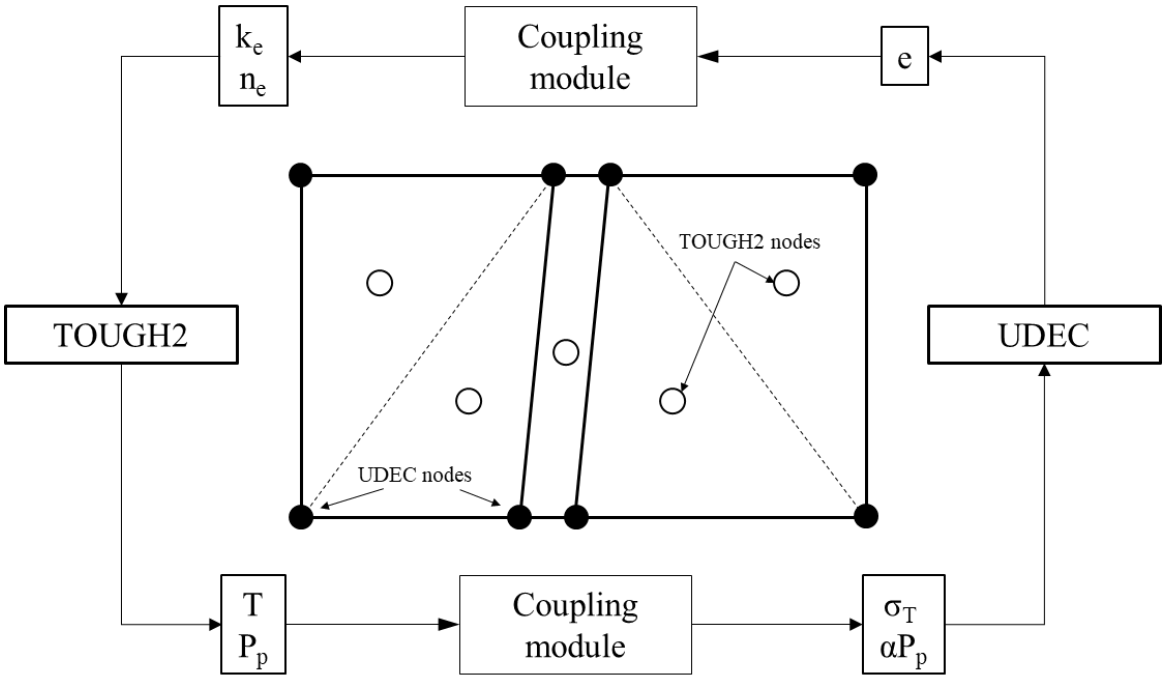

Fig. 2. A flow diagram of the TOUGH–UDEC coupling procedure.

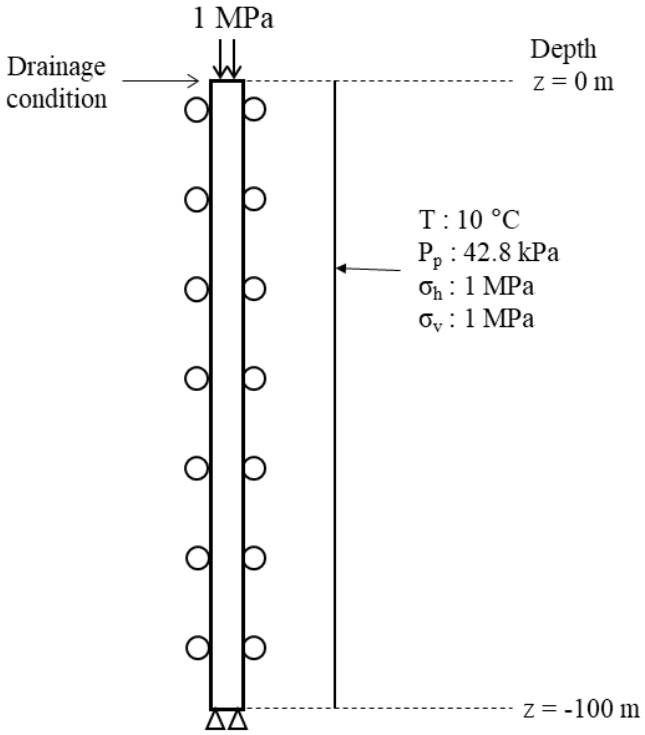

Fig. 3. A schematic view of the model geometry and boundary condition of uniaxial consolidation

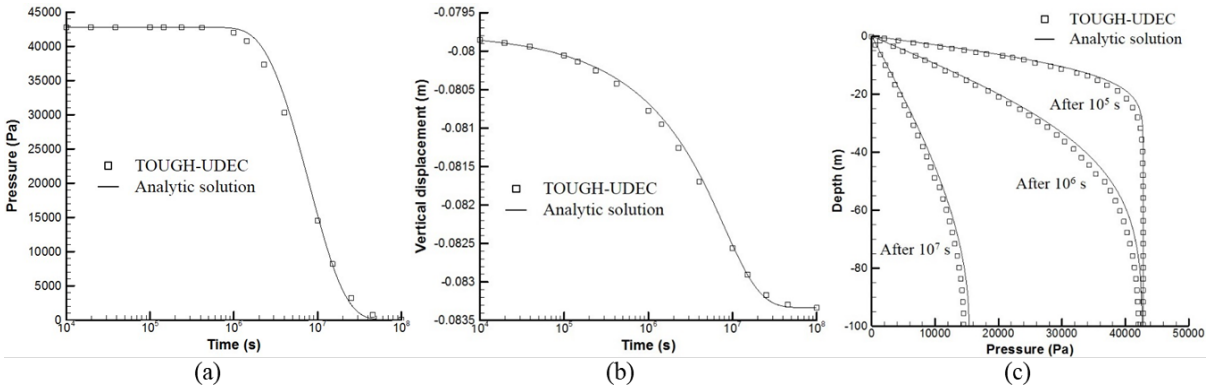

Fig. 4. Evolution of the (a) pressure at the lower boundary and (b) displ acement at the upper boundary, and (c) Pressure distributions after 10^5, 1 0^6, and 10^7 seconds

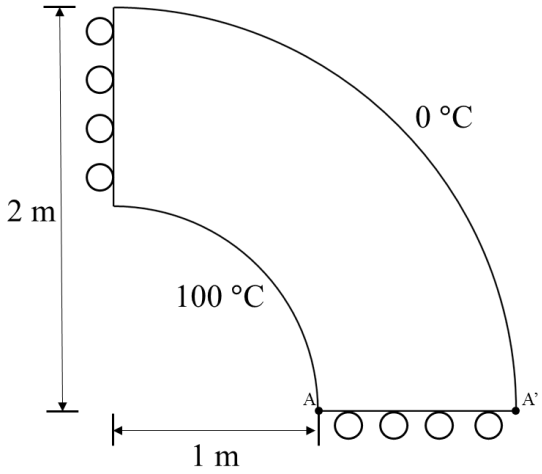

Fig. 5. Geometry and boundary conditions of a quarter section of the hol low cylinder model

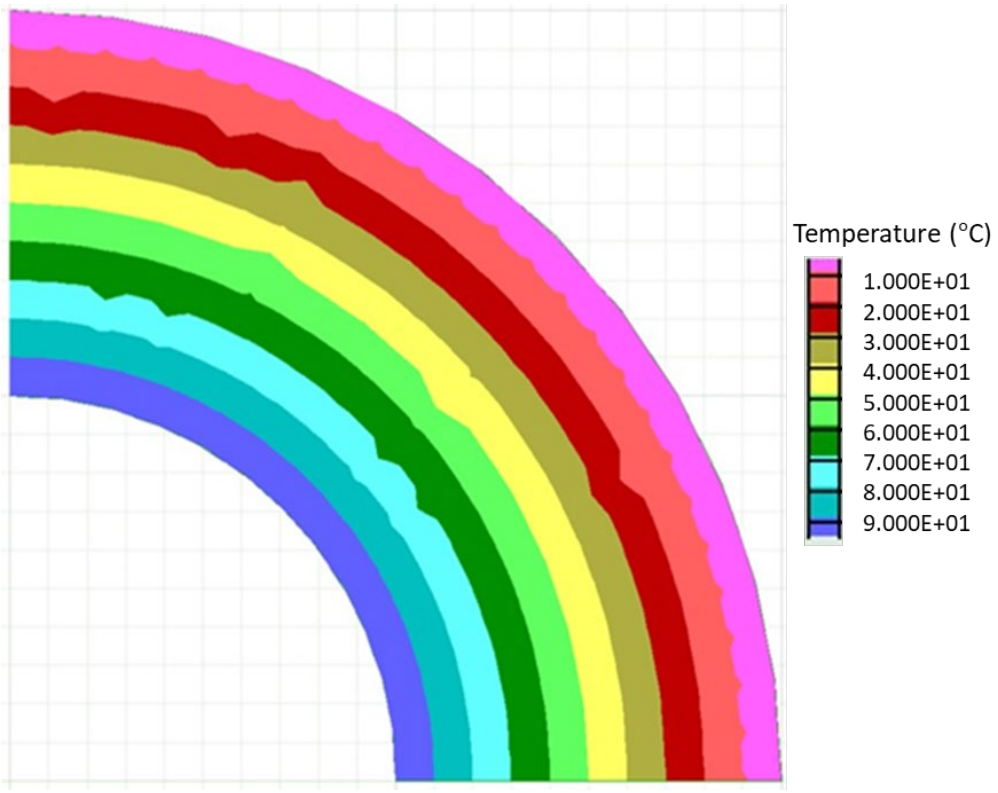

Fig. 6. Temperature contour of the model in a steady state

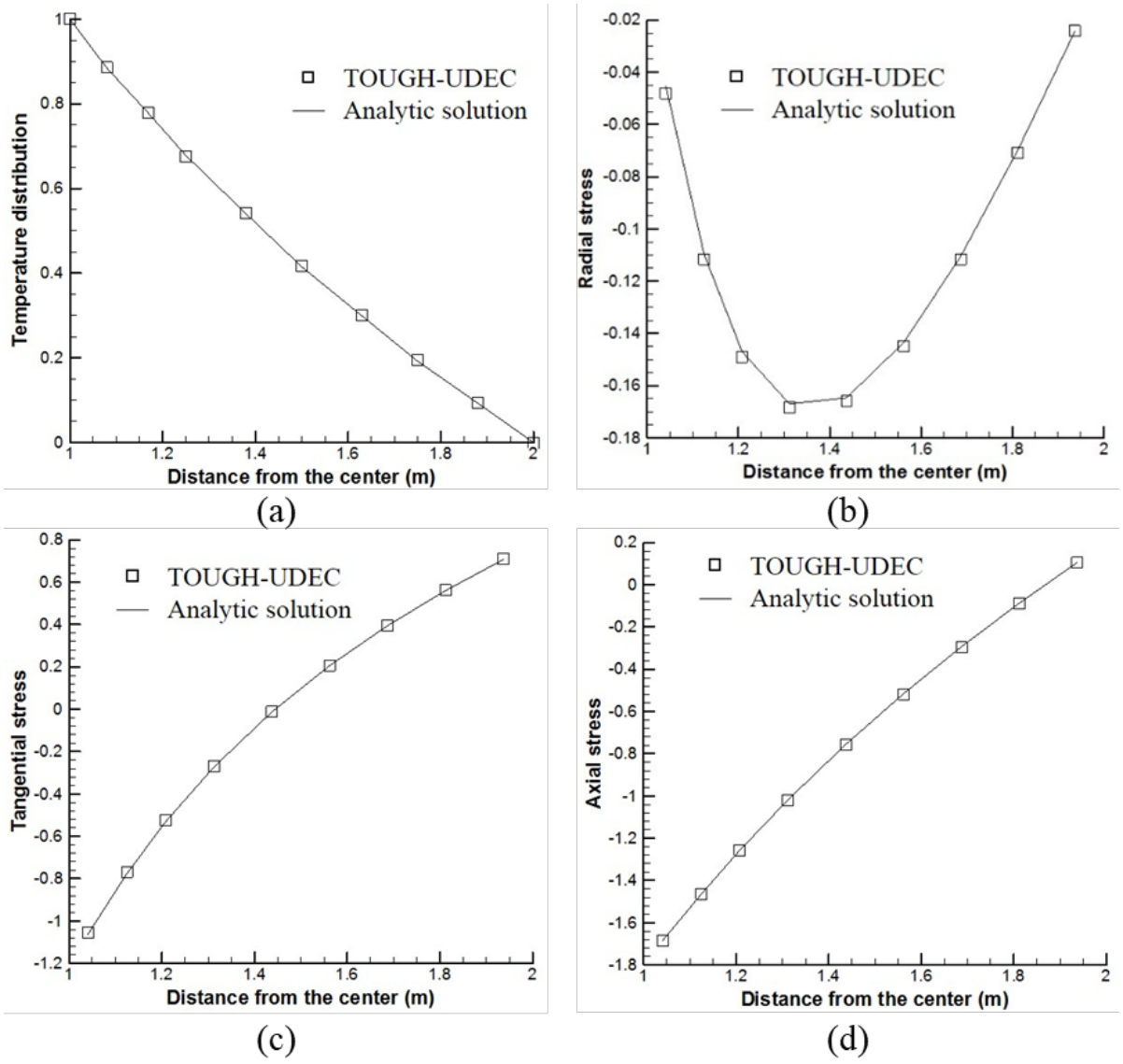

Fig. 7. (a) Temperature, (b) radial stress, (c) tangential stress, and (d) axi al stress distribution along the radial axis compared with the analytic solu tions

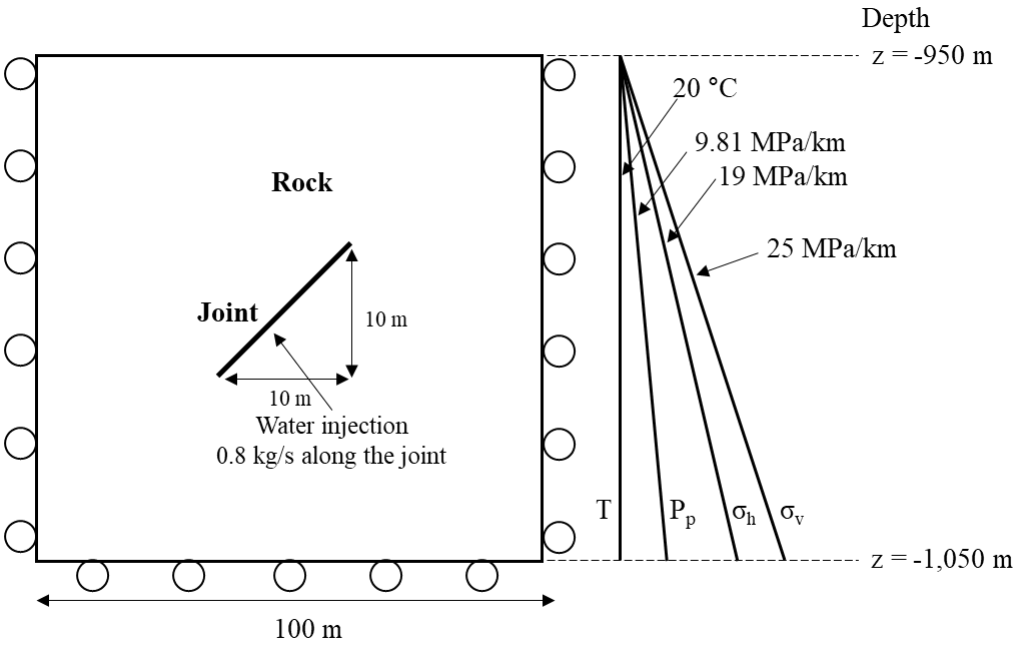

Fig. 8. Schematic view of a single inclined joint model with a fluid injec tion

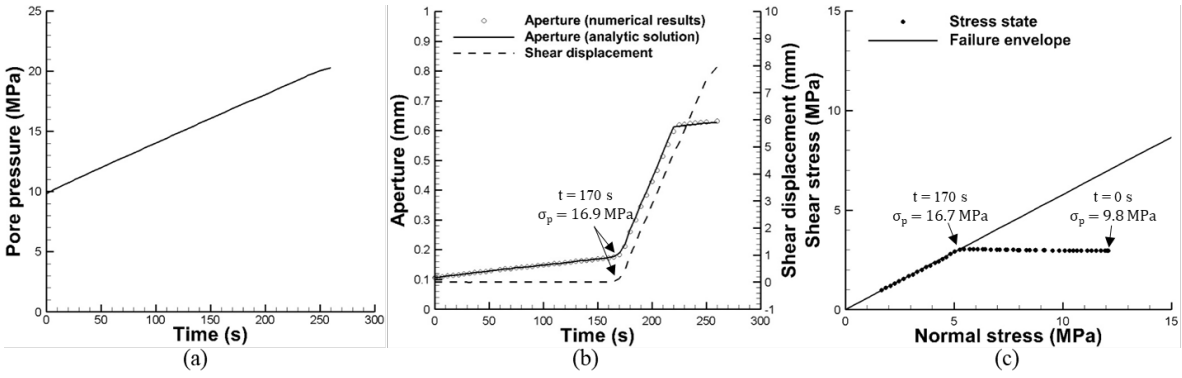

Fig. 9. Variations of the (a) pore pressure, (b) aperture and shear displace ment, and (c) stress state at the center of the joint

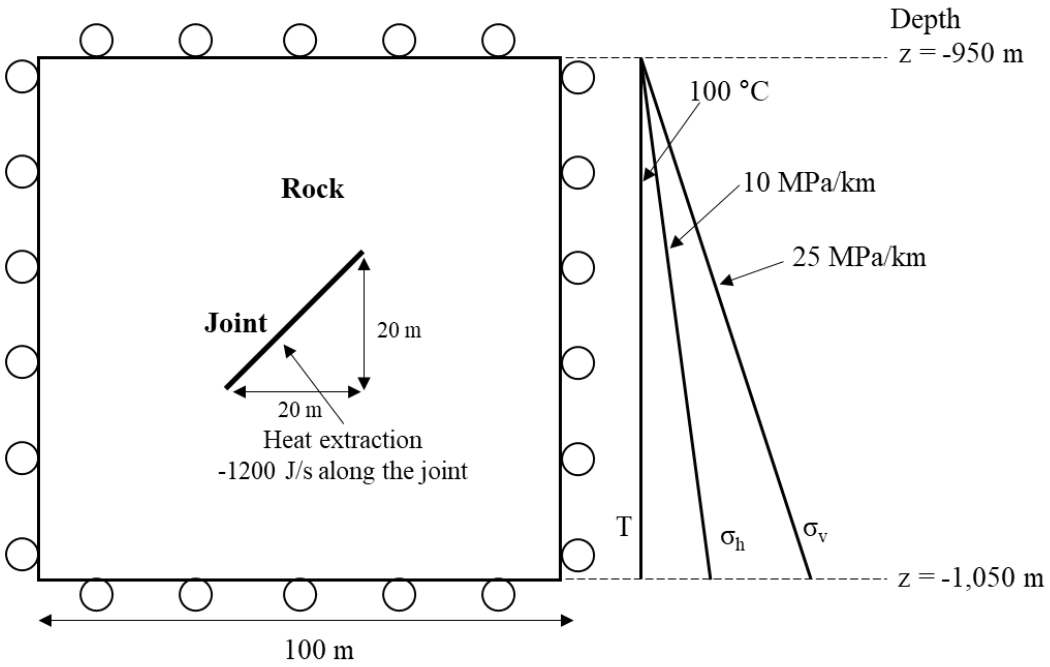

Fig. 10. Schematic view of a single-inclined-fracture model with heat extr action

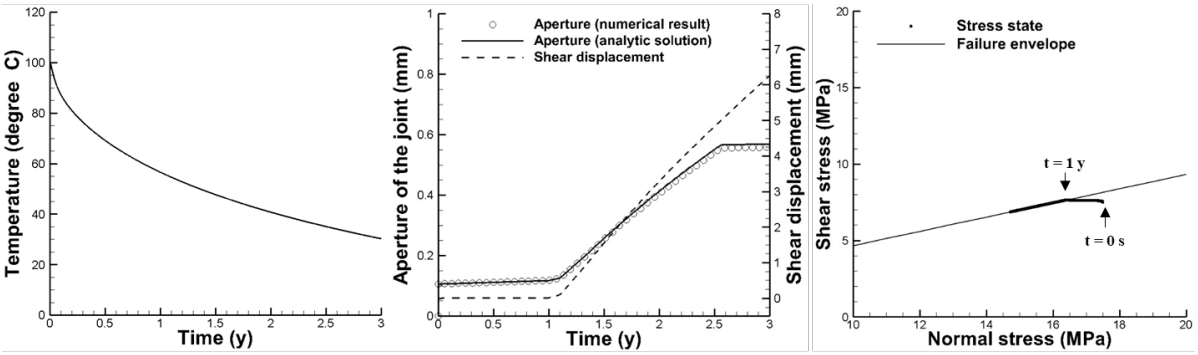

(a) (b) (c)

Fig. 11. Variations of (a) temperature (b) aperture and shear displacement, and (c) stress state at the center of the joint

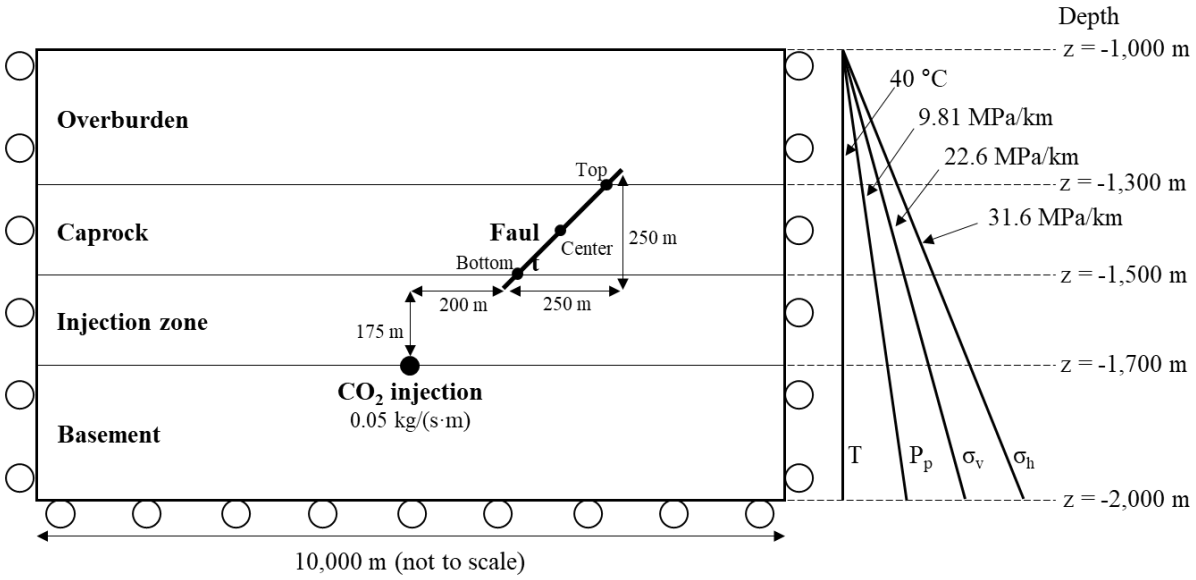

Fig. 12. Schematic view of a brine formation model for CO_2 geosequestration with initial and boundary conditions.

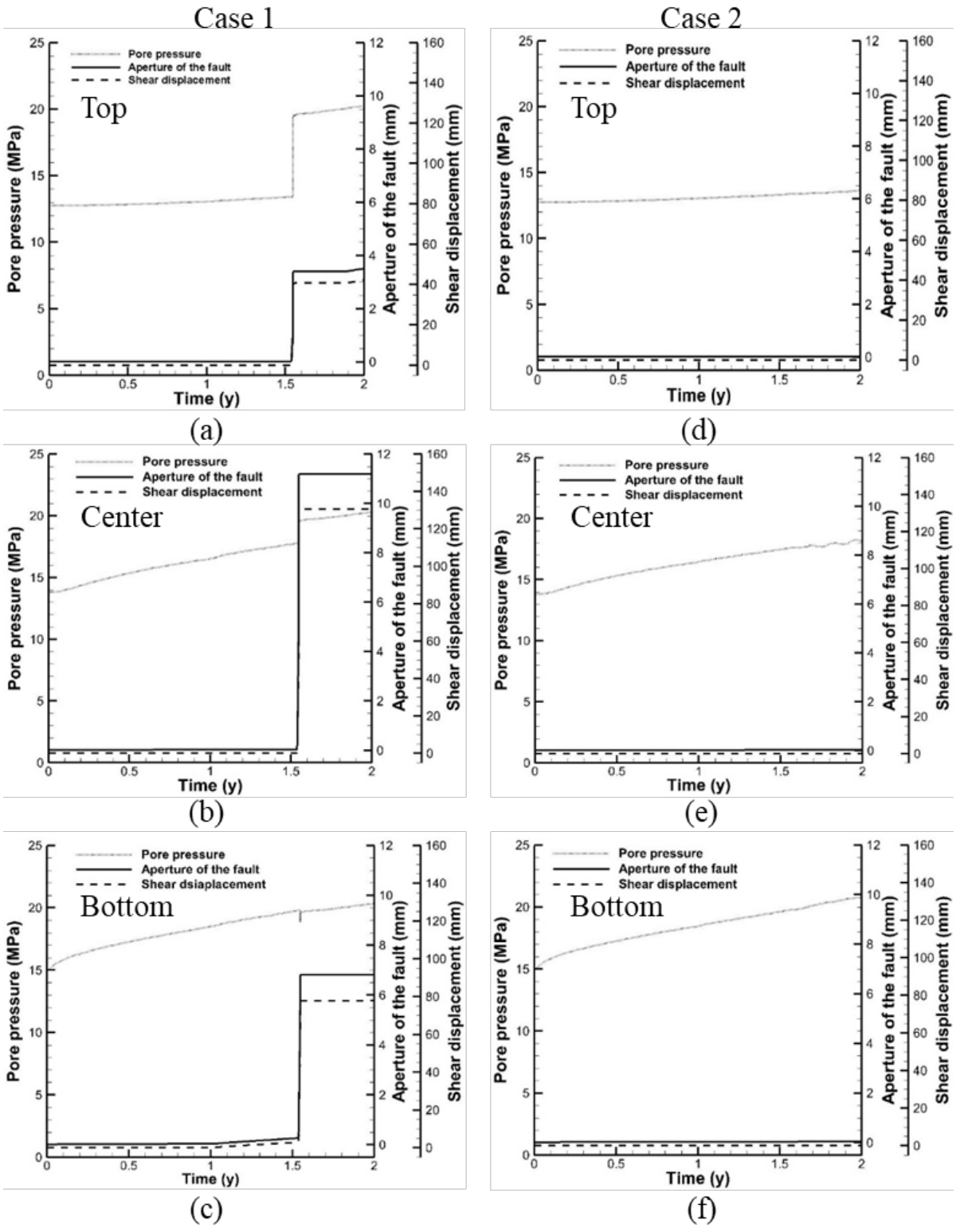

Fig. 13. Pore pressure, aperture of the fault, and shear displacement at th e top, center, and bottom of the fault for case 1 ((a), (b), and (c)) and c ase 2 ((d), (e), and (f))

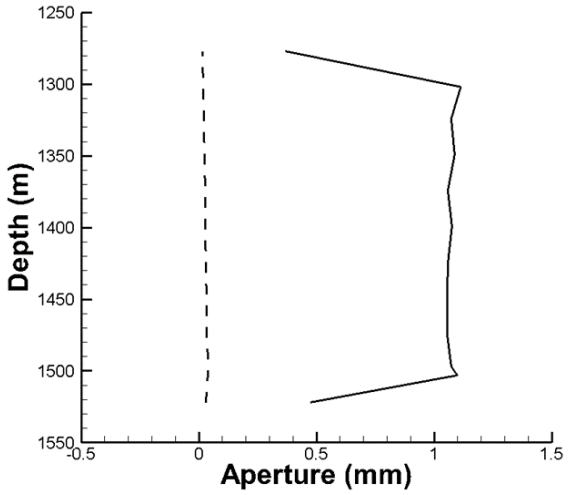

Fig. 14. Aperture profiles along the depth of the fault after two years of injection for cases 1 (solid) and 2 (dashed)

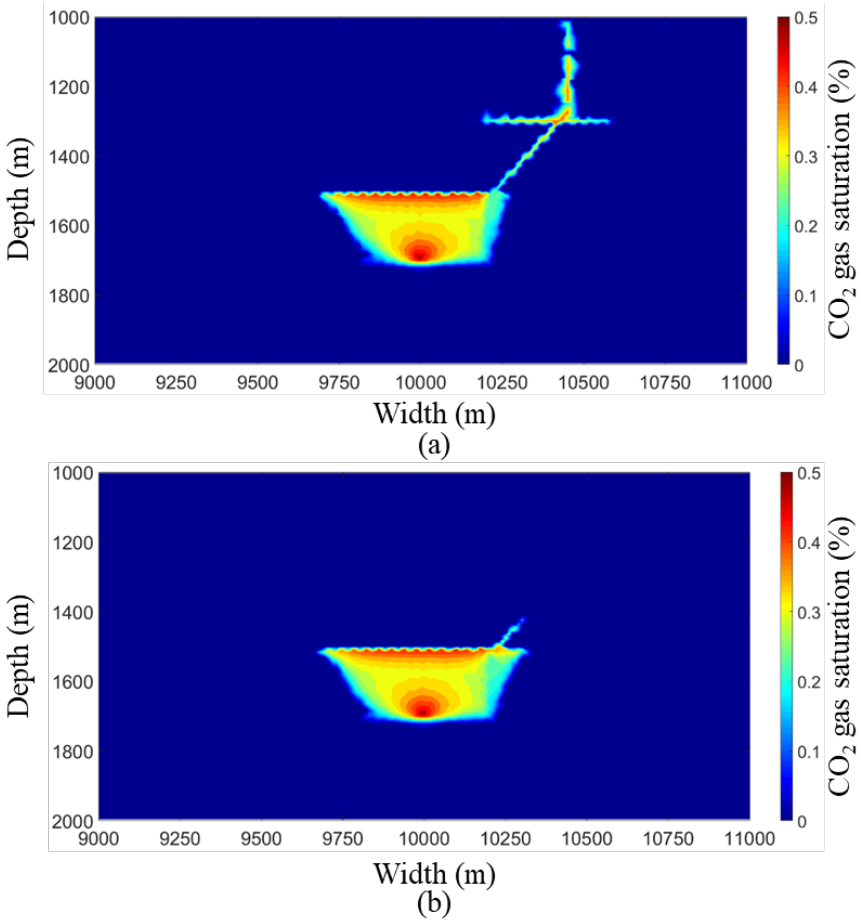

Fig. 15. CO_2 gas saturation contours of (a) case 1 and (b) case 2 after two years of injectio

Table 1. Properties of the model for the uniaxial consolidation analysis

Property	Value
Biot constant (–)	1.0
Permeability (m^2)	1×10^{-14}
Porosity (–)	0.1
Rock density (kg/m^3)	2,500
Bulk modulus (GPa)	0.667
Shear modulus (GPa)	0.4
Biot's modulus (–)	5.33×10^{8}

Table 2. Properties of the hollow cylinder model

Property	Value
Density (kg/m^3)	2,000
Specific heat (J/kg °C)	880
Thermal conductivity (W/m °C)	4.2
Thermal expansion coefficient (/ °C)	5.4×10^{-6}
Bulk modulus (GPa)	48
Shear modulus (GPa)	28

Table 3. Properties of the model of fluid injection for a single-inclined-fracture model

Property	Value
Bulk modulus (GPa)	3.33
Shear modulus (GPa)	2.0
Permeability of rock (m^2)	10^{-17}
Initial aperture of the joint (m)	1.06×10^{-4}
Friction coefficient (–)	0.577
Dilation angle (°)	5
Joint normal stiffness (GPa/m)	100
Joint shear stiffness (GPa/m)	10
Critical shear displacement for dilation (m)	5.0×10^{-3}

Table 4. Properties of the model of heat extraction around a single inclined fracture

Property	Value
Density (kg/m^3)	2,260
Bulk modulus (GPa)	3.33
Shear modulus (GPa)	2.0
Permeability of rock (m^2)	10^{-17}
Specific heat (J/kg °C)	1,500
Thermal conductivity (W/m °C)	1.8
Thermal expansion coefficient (/ °C)	2.0×10^{-5}
Initial aperture of the joint (m)	1.06×10^{-4}
Friction coefficient (–)	0.466
Dilation angle (°)	5.0
Fracture normal stiffness (GPa/m)	100
Fracture shear stiffness (GPa/m)	10
Critical shear displacement for dilation (m)	5.0×10^{-3}

Table 5. Material properties of the brine formation used for CO_2 geosequestration (Rutqvist et al., 2002)

Property	Overburden	Caprock	Injection zone	Basement
Elastic modulus (GPa)	5	5	5	5
Poisson's ratio (-)	0.25	0.25	0.25	0.25
Density (kg/m^3)	2260	2260	2260	2260
Porosity (-)	0.1	0.01	0.1	0.01
Permeability (m^2)	1×10^{-15}	1×10^{-17}	1×10^{-13}	1×10^{-17}
Corey's irreducible gas saturation (-)	0.05	0.05	0.05	0.05
Corey's irreducible liquid saturation	0.3	0.3	0.3	0.3
van Genuchten's air-entry pressure (kPa)	19.6	3,105	19.6	3,105
van Genuchten's exponent (-)	0.457	0.457	0.457	0.457

Table 6. Material properties of the fault in the two cases used for CO_2 injection and leakage analysis

Property	Case 1	Case 2
Normal stiffness (GPa/m)	200	200
Shear stiffness (GPa/m)	20	20
Static friction angle (°)	20	40
Residual friction angle (°)	15	35
Dilation angle (°)	5	5
Initial aperture of the joint (m)	1.06×10^{-5}	1.06×10^{-5}
Critical shear displacement for dilation (m) (McClure and Horne, 2014)	2.0×10^{-2}	2.0×10^{-2}